Korean J. Chem. Eng., **30**(4), 963-975 (2013)
DOI: 10.1007/s11814-012-0216-8

Comparisons of particle cluster diameter and concentration in circulating fluidized bed riser and downer using computational fluid dynamics simulation

Benjapon Chalermsinsuwan*,,†, Dimitri Gidaspow***, and Pornpote Piumsomboon*,****

*Fuels Research Center, Department of Chemical Technology, Faculty of Science, Chulalongkorn University, 254 Phayathai Road, Patumwan, Bangkok 10330, Thailand
**Center of Excellence on Petrochemical and Materials Technology, Chulalongkorn University, 254 Phayathai Road, Patumwan, Bangkok 10330, Thailand
***Department of Chemical and Biological Engineering, Illinois Institute of Technology, Chicago, IL 60616, U.S.A.
(*Received 28 July 2012 • accepted 16 December 2012*)

Abstract−The information of particle cluster dynamics is necessary for improving the performance of a circulating fluidized bed system. The main objective of this study is to compare the particle cluster diameters and concentrations from computational fluid dynamics simulation results between circulating fluidized bed riser and downer. The calculation methodologies are based on the concept of kinetic theory of granular flow and statistics. The mathematical model was verified by using the experimental dataset from literature and used for computing the particle cluster dynamics. In the circulating fluidized bed riser and downer, a dense and dilute core-annulus flow structures were obtained, respectively. The particle cluster in the circulating fluidized bed riser possessed more heterogeneity movements than that in the circulating fluidized bed downer. This can be explained by the system flow direction. About the particle cluster dynamics, the particle cluster diameters and concentrations in the circulating fluidized bed riser were higher than the ones in the downer. The calculated values were comparable to the empirical correlations. This confirms the validity of the calculation methodologies. Particle cluster dynamics and its example application inside circulating fluidized bed riser and downer were also discussed.

Key words: Circulating Fluidized Bed, Computational Fluid Dynamics, Downer, Particle Cluster, Riser, Simulation

INTRODUCTION

The design of a circulating fluidized bed (CFB) reactor for use in various industrial scale applications, such as combustor and gasifier, requires knowledge of system hydrodynamics. Typically, the CFB consists of two major reaction components, riser and downer. For both risers and downers, a core-annulus system flow pattern was observed [1,2]. The solid particles are dense and dilute near the wall and center regions, respectively. At the annulus or wall region, the solid particles then agglomerate and form as particle clusters. One key feature of the system hydrodynamics behavior in CFB is the existence of particle clusters. The particle cluster flow structure is significantly different from the individual solid particles [3]. When particle clusters form in a CFB, they affect the overall gas-solid system flow behaviors. Therefore, information about the particle cluster characteristics is necessary. In the experiment, it is known that the particle cluster prohibits a good multiphase mixing inside the system [4]. This then has negative effect on the system chemical reaction conversion. By the computational fluid dynamics (CFD) simulation, the particle cluster information can be obtained and used for the calculation of drag or interphase exchange coefficient models. The particle cluster size was substituted in the correlations instead of the solid particle size until the correct system hydrodynamics were obtained [5-7]. In addition, it can be employed in computing the mass transfer coefficient, which is then used as an input parameter for the conventional shrinking core chemical reaction model [8,9]. The mass transfer coefficient is one of the three resistances along with diffusion and chemical reaction. In the literature, the mass transfer coefficient is recognized to be much lower for small particles than that given by conventional correlations for large particles [10,11]. Chalermsinsuwan et al. [12] explained this situation by the formation of particle cluster inside their CFB riser. Still, no data is reported on the CFB downer.

The particle cluster or aggregate is a group of solid particles defined as regions with high solid particle concentration in relation to the mean concentration [13]. These groups of particles move as a single body with little internal relative movement [14]. These aggregates play a major role in all flow development length, axial and radial dispersions near the wall, heat and mass transfers near the wall, and thus affect the overall performance of a CFB reactor [15]. Nevertheless, the way to identify and characterize two important parameters of particle cluster for use in the CFD simulation aspects, which are diameter and concentration, is still in a development stage. Most of the previous literature studies are focused on the calculation of the other particle cluster dynamics, such as mean duration time, frequency of occurrence, existence time fraction and particle cluster number, which are the necessary parameters for use in the experiment aspects [16-18].

The study about the particle cluster was initiated by Yerushalmi et al. [19], who proposed a hypothesis on particle cluster formation. Gidaspow et al. [20] conducted both the experiment and simulation

†To whom correspondence should be addressed.
E-mail: benjapon.c@chula.ac.th

to visualize the trajectories of particle clusters near wall region of their CFB riser. Horio and Kuroki [21], Tartan and Gidaspow [22], Jung et al. [23] and Xu and Zhu [24] found the existence of particle clusters in the fluidized bed (FB) and CFB riser system operations. They observed the heterogeneity movements of particle clusters (downward, stagnant and upward). Zhang et al. [25] simulated the particle cluster behaviors in a CFB riser and downer. They stated that there were two types of particle cluster, one in the near wall region and the other one in the center region. As the formation of particle clusters is widely recognized, the information on how to identify and characterize them is mostly limited. For the parameters used in the experimental aspect, Soong et al. [26] developed criteria using a statistical methodology to identify particle cluster dynamics based on their experimental data in a CFB riser. As mentioned above, those dynamics were the mean duration time, frequency of occurrence and existence time fraction. Sharma et al. [27] used the same methodology as Soong et al. [26] to obtain the effects of operating conditions on those dynamics. In addition, the methodology was validated for use in the CFD simulation results as shown in Gómez et al. [28]. For the parameters used in the CFD simulation aspect, Chalermsinsuwan et al. [12] successfully calculated the particle cluster diameter and concentration in a CFB riser using the kinetic theory of granular flow [29] and statistical concepts [26]. Breault [30] analyzed the clustering flows in a CFB riser using Gibbs free energy. Their Gibbs free energy was related to the particle cluster size. The computed values of their particle cluster dynamics were in agreement with their previous experimental results [31]. Besides the above studies, only the empirical correlations of particle cluster diameter and concentration from the experimental data were proposed [32-35].

We used the kinetic theory of granular flow and statistical concepts to calculate the particle cluster diameters and concentrations from CFD simulation results. This is the information still lacking in the literature. The methodology was applied to both the CFB riser and downer as experimented by Knowlton et al. [36] and Cao and Weinstein [37]. This is because the experimental validation was used as a method for verifying the results. Then, the obtained values were compared with each other and with the estimated values from the empirical correlations. In addition, the particle cluster dynamics and example application were discussed.

COMPUTATIONAL FLUID DYNAMICS SIMULATIONS

1. Mathematical Models

In this study, the CFD simulation was solved by using the commercial ANSYS FLUENT 6.3.26 program. There are two main mathematical models for multiphase flow available in the program: the Lagrangian model and the Eulerian model. In these CFB riser and downer systems, the Eulerian model was selected because the solid phase quantity cannot be occupied by the gas phase one [38]. With this model, conservation equations, mass and momentum, for each phase were considered to be continuous and fully inter-penetrating. Both phases were described in terms of separate sets of conservation equations with their appropriate interaction terms representing the coupling between the phases. The equations were closed by providing constitutive equations based on the kinetic theory of granular flow. The kinetic theory of granular flow is an extension of the conventional kinetic theory of gases by adding the effects of solid particle collision and solid fluctuating kinetic energy (or granular temperature). More information about this theory is provided in Gidaspow [29]. The verification of the employed model was already proved in our previous studies with the same CFB riser [12] and downer [39] systems. For the CFB riser, Chalermsinsuwan et al. [12] vali-

Table 1. A summary of the conservation equations and constitutive equations

A. Governing equations;

(a) Conservation of mass;

(a) Gas phase;

$$\frac{\partial}{\partial t}(\varepsilon_g\rho_g)+\nabla\cdot(\varepsilon_g\rho_g\vec{v}_g)=0 \quad (1)$$

(b) Solid phase;

$$\frac{\partial}{\partial t}(\varepsilon_s\rho_s)+\nabla\cdot(\varepsilon_s\rho_s\vec{v}_s)=0 \quad (2)$$

(b) Conservation of momentum;

(a) Gas phase;

$$\frac{\partial}{\partial t}(\varepsilon_g\rho_g\vec{v}_g)+\nabla\cdot(\varepsilon_g\rho_g\vec{v}_g\vec{v}_g)=-\varepsilon_g\nabla p+\nabla\cdot\tau_g+\varepsilon_g\rho_g g-\beta_{gs}(\vec{v}_g-\vec{v}_s) \quad (3)$$

(b) Solid phase;

$$\frac{\partial}{\partial t}(\varepsilon_s\rho_s\vec{v}_s)+\nabla\cdot(\varepsilon_s\rho_s\vec{v}_s\vec{v}_s)=-\varepsilon_s\nabla p+\nabla\cdot\tau_s-\nabla p_s+\varepsilon_s\rho_s g+\beta_{gs}(\vec{v}_g-\vec{v}_s) \quad (4)$$

(c) Conservation of solid phase fluctuating energy;

$$\frac{3}{2}\left[\frac{\partial}{\partial t}(\varepsilon_s\rho_s\theta)+\nabla\cdot(\varepsilon_s\rho_s\theta)\vec{v}_s\right]=(-\nabla p_s\bar{I}+\tau_s):\nabla\vec{v}_s+\nabla\cdot(\kappa_s\nabla\theta)-\gamma_s \quad (5)$$

B. Constitutive equations;

(a) Gas phase stress;

$$\tau_g=\varepsilon_g\mu_g[\nabla\vec{v}_g+(\nabla\vec{v}_g)^T]-\frac{2}{3}\varepsilon_g\mu_g(\nabla\cdot\vec{v}_g)I \quad (6)$$

Table 1. Continued

(b) Solid phase stress;

$$\tau_s = \varepsilon_s \mu_s [\nabla \vec{v}_s + (\nabla \vec{v}_s)^T] - \varepsilon_s \left(\xi_s - \frac{2}{3} \mu_s \right) \nabla \cdot \vec{v}_s \mathrm{I} \tag{7}$$

(c) Collisional dissipation of solid phase fluctuating energy;

$$\gamma_s = 3(1-e^2) \varepsilon_s^2 \rho_s g_0 \theta \left(\frac{4}{d} \sqrt{\frac{\theta}{\pi}} \right) \tag{8}$$

(d) Conductivity of the solid phase fluctuating energy;

$$\kappa_s = \frac{150 \rho_s d_p \sqrt{\theta \pi}}{384(1+e) g_0} \left[1 + \frac{6}{5} \varepsilon_s g_0 (1+e) \right]^2 + 2 \rho_s \varepsilon_s^2 d_p (1+e) g_0 \sqrt{\frac{\theta}{\pi}} \tag{9}$$

(e) Radial distribution function;

$$g_0 = \left[1 - \left(\frac{\varepsilon_s}{\varepsilon_{s,max}} \right)^{1/3} \right]^{-1} \tag{10}$$

(f) Solid phase shear viscosity;

$$\mu_s = \frac{4}{5} \varepsilon_s \rho_s d_p g_0 (1+e) \sqrt{\frac{\theta}{\pi}} + \frac{10 \rho_s d_p \sqrt{\pi \theta}}{96(1+e) g_0 \varepsilon_s} \left[1 + \frac{4}{5} g_0 \varepsilon_s (1+e) \right]^2 \tag{11}$$

(g) Solid phase bulk viscosity;

$$\xi_s = \frac{4}{3} \varepsilon_s \rho_s d_p g_0 (1+e) \sqrt{\frac{\theta}{\pi}} \tag{12}$$

(h) Solid phase pressure;

$$p_s = \varepsilon_s \rho_s \theta [1 + 2 g_0 \varepsilon_s (1+e)] \tag{13}$$

(i) Gas and solid phases interphase exchange coefficient;

- EMMS model;

when $\varepsilon_g < 0.74$;

$$\beta_{gs} = 150 \frac{(1-\varepsilon_g)^2 \mu_g}{\varepsilon_g d_p^2} + 1.75 \frac{(1-\varepsilon_g) \rho_g |\vec{v}_g - \vec{v}_s|}{d_p} \tag{14}$$

when $\varepsilon_g \geq 0.74$;

$$\beta_{gs} = \frac{3}{4} \frac{(1-\varepsilon_g) \varepsilon_g}{d_p} \rho_g |\vec{v}_g - \vec{v}_s| C_{D0} \omega(\varepsilon) \tag{15}$$

- Gidaspow model;

when $\varepsilon_g \leq 0.80$;

$$\beta_{gs} = 150 \frac{(1-\varepsilon_g)^2 \mu_g}{\varepsilon_g d_p^2} + 1.75 \frac{(1-\varepsilon_g) \rho_g |\vec{v}_g - \vec{v}_s|}{d_p} \tag{16}$$

when $\varepsilon_g > 0.80$;

$$\beta_{gs} = \frac{3}{4} \frac{(1-\varepsilon_g) \varepsilon_g}{d_p} \rho_g |\vec{v}_g - \vec{v}_s| C_{D0} \varepsilon_g^{-2.65} \tag{17}$$

with

$\mathrm{Re} < 1000$; $C_{D0} = \frac{24}{\mathrm{Re}_k}(1 + 0.15 \mathrm{Re}_k^{0.687})$; $\mathrm{Re}_k = \frac{\rho_g \varepsilon_g |\vec{v}_g - \vec{v}_s| d_p}{\mu_g}$

$\mathrm{Re} \geq 1000$; $C_{D0} = 0.44$

when $0.74 \leq \varepsilon_g \leq 0.82$; $\omega(\varepsilon) = -0.5760 + \frac{0.0214}{4(\varepsilon_g - 0.7463)^2 + 0.0044}$

when $0.82 \leq \varepsilon_g \leq 0.97$; $\omega(\varepsilon) = -0.0101 + \frac{0.0038}{4(\varepsilon_g - 0.7789)^2 + 0.0040}$

when $\varepsilon_g > 0.97$; $\omega(\varepsilon) = -31.8295 + 32.8295 \varepsilon_g$

(j) Wall tangential velocity and granular temperature of the solid phase (Jackson and Johnson boundary condition);

$$\vec{v}_{t,W} = -\frac{6 \mu_s \varepsilon_{s,max}}{\pi \phi \rho_s \varepsilon_s g_0 \sqrt{3\theta}} \frac{\partial \vec{v}_{s,W}}{\partial n} \tag{18}$$

$$\theta_W = -\frac{\kappa_s}{\gamma_W} \theta \frac{\partial \theta_W}{\partial n} + \frac{\sqrt{3} \pi \phi \rho_s \varepsilon_s \vec{v}_{s,slip}^2 g_0 \theta^{3/2}}{6 \varepsilon_{s,max} \gamma_W} \tag{19}$$

with $\gamma_W = \frac{\sqrt{3} \pi (1 - e_W^2) \varepsilon_s \rho_s g_0 \theta^{3/2}}{4 \varepsilon_{s,max}}$

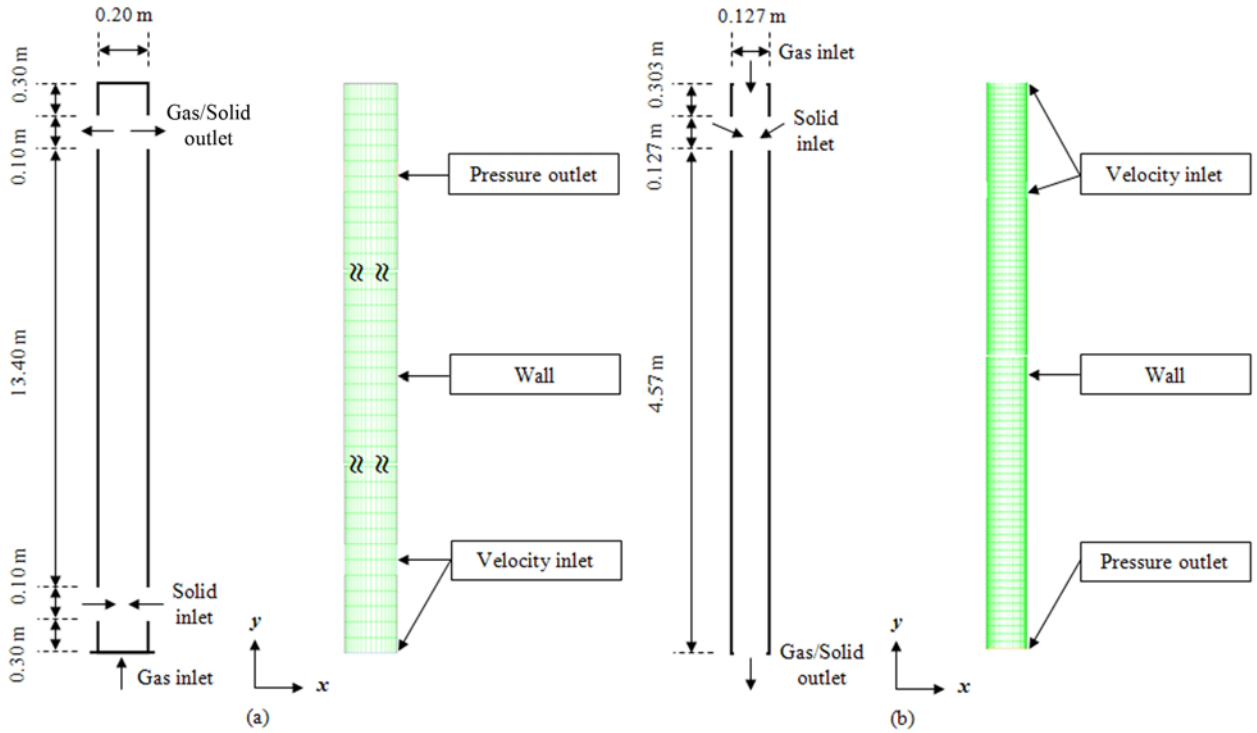

Fig. 1. Schematic drawing and computational domain with their boundary conditions of simplified CFB (a) riser and (b) downer.

dated the mathematical model with the solid mass flux, solid density and system pressure drop profiles. For the CFB downer, Chalermsinsuwan et al. [39] validated the mathematical model with the solid volume fraction, solid mass flux and gauge pressure profiles. Also, the effects of various modeling parameters were explained in their study, such as the restitution coefficient, specularity coefficient, interphase exchange coefficient model and turbulence model. The chosen models were the best appropriate ones with the literature experimental data [36,37]. Therefore, the verification steps were skipped and the mathematical models were used for further analyzing the particle cluster dynamics. A summary of the conservation equations and constitutive equations is given in Table 1. The main difference between the models of CFB riser and downer was the drag coefficient correlations. In case of high solid mass flux system/CFB riser, the energy minimization multi-scale (EMMS) drag coefficient model was suitable to employ, while in case of low solid mass flux system/CFB downer, the Gidaspow drag coefficient model was used [40-42]. For the CFB riser, the new additional code using VISUAL C++ programming language was added because the EMMS drag coefficient model was not provided in the program.

2. System Descriptions and Computational Domains

To compare the particle cluster diameters and concentrations, the experimental results by Knowlton et al. (for the CFB riser) [36] and Cao and Weinstein (for the CFB downer) [37] were chosen as the two reference cases. In the literature, there is little reported experimental data for both the riser and downer in the same CFB system. Therefore, two different experimental data with the same Geldart classification were selected as each CFB section's representative to simulate and explain in this study.

For the CFB riser condition, the gas in their system was pure air with 1.20 kg/m^3 in density and 2.00×10^{-5} kg/m s in viscosity. The solid particles in their system were fluid catalytic cracking (FCC) with 76 mm in diameter and 1,712 kg/m^3 in density. The diameter and height of their CFB riser were 0.20 m and 14.20 m, respectively. Since the three-dimensional model requires long computation time, we used the two-dimensional model for the simulation. The schematic drawing of the CFB riser is depicted in Fig. 1(a). This schematic drawing is based on Benyahia et al. [43] and Chalermsinsuwan et al. [12], which was a two inlet-outlet design for the two-dimensional CFB riser. This is because a one inlet-outlet design for two-dimensional CFB riser cannot capture the system phenomena [12]. The gas was fed to the system at the bottom of the CFB riser. The solid particles were fed from the two side inlets at 0.30 m above the bottom of the system with a width of 0.10 m. The gas and solid particles exited the system through two side outlets at 0.30 m below the top of the CFB riser (similar width to the side inlets).

For the CFB downer condition, the gas was also air with 1.20 kg/m^3 in density and 2.00×10^{-5} kg/m s in viscosity. The solid particles in their system were FCC particles. However, their physical properties were slightly changed. The solid particle diameter and density were 82 mm and 1,480 kg/m^3. With these properties, the same group A in Geldart classification was still obtained. The diameter and height of their CFB downer was 0.127 m and 5.00 m, respectively. Similar to the CFB riser, this we used the two-dimensional model for the simulation. The schematic drawing of the CFB downer, depicted in Fig. 1(b), is based on Chalermsinsuwan et al. [39], which is a two inlet design for the two-dimensional CFB downer. The gas was fed to the system at the top of the CFB downer. The solid particles were fed from the 0.127 m width two side inlets at 0.303 m below the top of the system with the angle of 45° with respect to the system vertical (y) axis. The gas and solid particles exited through the system outlet at the bottom of the CFB downer.

The computational domains of the CFB riser and downer in this study with their corresponding boundary conditions are also illustrated in Figs. 1(a) and 1(b), respectively. For both the CFB systems, the computational domain consisted of 20 non-uniform grids in radial or horizontal direction and 300 uniform grids in axial or vertical direction, with a total of 6,000 computational cells. The CFD models were solved by using a personal computer with Pentium 1.80 GHz CPU 1 GB RAM. It took approximately 5 days of computation time for 50 s of simulation time. The time-averaged quasi-steady state results were calculated using the results with the simulation time in the range of 30 s to 50 s. For these two CFB systems, the grid independence study and time-averaged range checking were already tested [12,39]. The acceptable results should not depend on the grid size and simulation time. Chalermsinsuwan et al. [12,39] performed the CFD simulation with the increments of grid size and the simulation time in CFB riser and downer, respectively. They obtained satisfactory values for both the parameters, as already summarized above.

3. Initial and Boundary Conditions

Initially, no gas phase and solid phase were packed in the CFB system. Thus, there was no solid holdup or solid volume fraction inside the system. At the system inlets, the velocities and volume fractions for each phase were specified to be consistent with the solid mass flux in the CFB riser and downer of 489 kg/m^2 s and 123 kg/m^2 s, respectively. Generally, the solid mass flux has a relationship with the solid density, solid volume fraction and solid velocity. For the selected CFB riser [36], this system was used for fluid catalytic cracking application. For the chosen CFB downer [37], the system was used only as a solid particle transportation part. The volume fraction and solid mass flux in the CFB downer were then lower than the CFB riser one. On the other hand, the system pressures were specified at the system outlets as input parameters for the CFD solving algorithm. At the system wall, no-slip boundary conditions were applied for all velocities, except the tangential velocity of solid phase and fluctuating kinetic energy of solid phase, which were used the boundary conditions of Johnson and Jackson [44]. All the used parameter values for the simulation are listed in Table 2. The employed modeling parameters were selected from the suitable ones in our previous studies [12,39].

RESULTS AND DISCUSSION

1. Calculation Methodology for Particle Cluster Diameter

As already stated, we used the methodology from Chalermsinsuwan et al. [12]. Based on the kinetic theory of granular flow concept [29], the description of particle cluster diameter is the radial characteristic length of solid particle, which can be obtained by dividing the radial solid dispersion coefficient at any radial system distance ($D_x(r)$) with the radial oscillating velocity:

$$\text{Particle cluster diameter} = \frac{D_x(r)}{\text{Radial oscillating velocity}} \tag{20}$$

The radial solid dispersion coefficient can be computed from a mathematical relation between the radial normal Reynolds stress ($\overline{v_x'v_x'(r)}$) and the Lagrangian integral time scale (T_L) [12,45]:

$$D_x(r) = \overline{v_x'v_x'(r)}T_L \tag{21}$$

$$T_L = \int_0^{\infty} \frac{\overline{v'(t)v'(t+t')}}{\overline{v'^2}} dt' \tag{22}$$

With the radial normal Reynolds stress is the additional stress due to random velocity fluctuations (v′) from its mean values in radial direction:

$$\overline{v_x'v_x'(r)} = \frac{1}{m}\sum_1^m (v_{x,k}(r,t) - \overline{v}_x(r))(v_{x,k}(r,t) - \overline{v}_x(r)) \tag{23}$$

$$\overline{v}_x(r) = \frac{1}{m}\sum_1^m v_{x,k}(r,t) \tag{24}$$

The radial oscillating velocity can be obtained from the square root of the radial normal Reynolds stress:

$$\text{Radial oscillating velocity} = \sqrt{\overline{v_x'v_x'(r)}} \tag{25}$$

2. Calculation Methodology for Particle Cluster Concentration

Similar to the particle cluster diameter, we used statistical methodology proposed by Soong et al. [26] and Chalermsinsuwan et al.

Table 2. The used parameter values for the CFD simulation

Symbol	Description	CFB riser	CFB downer
-	System diameter (m)	0.20	0.127
-	System height (m)	14.20	5.00
ρ_g	Gas density (kg/m^3)	1.2	1.2
μ_g	Gas viscosity (kg /m s)	2×10^{-5}	2×10^{-5}
ρ_s	Solid particle density (kg/m^3)	1,712	1,480
d_p	Solid particle diameter (mm)	76	82
v_g	Gas inlet velocity (m/s)	5.20	3.70
v_s	Solid inlet velocity (m/s)	0.476	1.11
ε_s	Solid inlet volume fraction (-)	0.60	0.15
G_s	Solid mass flux (kg/m^2 s)	489	123
p	System outlet pressure (Pa)	101,325	116,325
e	Restitution coefficient between solid particles (-)	0.95	0.999
e_W	Restitution coefficient between solid particle and wall (-)	0.90	0.70
ϕ	Specularity coefficient (-)	0.50	0.001

[12] to identify and characterize the particle clusters. Their particle cluster definition is:

"The solid particle is accepted to be the particle cluster when the instantaneous solid volume fraction becomes higher than the time-averaged solid volume fraction plus two times the standard deviation (2σ)."

After the particle cluster is identified, the particle cluster concentration or volume fraction is computed as the sum of the time-averaged solid volume fractions ($\bar{\varepsilon}_{cl,i}$) for all the particle clusters over the total number of particle clusters (m) detected in the observation period:

$$\text{Particle cluster concentration} = \frac{\sum_1^m \bar{\varepsilon}_{cl,i}}{\text{m}} \tag{26}$$

3. Empirical Correlations for Particle Cluster Diameter and Concentration

Up to now, only a limited number of research studies have been reported about the methodology to compute or estimate the particle cluster diameter and concentration for using in the CFD simulation aspect.

The curve-fitting correlations from the experimental data for the particle cluster diameter ($\bar{d}_{cl}$) with various system parameters are summarized as shown below. In [33-35] they proposed that their correlations were in good agreement with the experimental measurements in the CFB riser.

$$\text{Zou et al. [33]; } \bar{d}_{cl} = 1.8543 d_p \left[\frac{\bar{\varepsilon}_s^{0.25}(1-\bar{\varepsilon}_s)^{-1.5}}{(1-\bar{\varepsilon}_s-\varepsilon_{mf})^{2.41}} \right]^{1.3889} + d_p \tag{27}$$

$$\text{Gu and Chen [34]; } \bar{d}_{cl} = d_p + (0.027 - 10 d_p)\bar{\varepsilon}_s + 32\bar{\varepsilon}_s^6 \tag{28}$$

$$\text{Harris et al. [35]; } \bar{d}_{cl} = \frac{\bar{\varepsilon}_s}{40.8 - 94.5\bar{\varepsilon}_s} \tag{29}$$

where d_p is the solid particle diameter, $\bar{\varepsilon}_s$ is the solid volume fraction and ε_{mf} is the solid volume fraction at minimum fluidization velocity (which in this study was set roughly as 0.40 using theoretical/experimental results by Benyahia et al. [1,43]).

Similar to particle cluster diameter, Lints and Glicksman [32], Gu and Chen [34] and Harris et al. [35] presented correlations for predicting the particle cluster concentration/volume fraction. Their correlations were developed from experimental data published in CFB riser publication ranging from laboratory to industrial scale.

$$\text{Lints and Glicksman [32]; } \bar{\varepsilon}_{cl} = \bar{\varepsilon}_s^{0.50} \tag{30}$$

$$\text{Gu and Chen [34]; } \bar{\varepsilon}_{cl} = \varepsilon_{s,max}\left[1 - \left(1 - \frac{\bar{\varepsilon}_s}{\varepsilon_{s,max}} \right)^{3.4} \right] \tag{31}$$

$$\text{Harris et al. [35]; } \bar{\varepsilon}_{cl} = \frac{0.58\bar{\varepsilon}_s^{1.48}}{0.013 + \bar{\varepsilon}_s^{1.48}} \tag{32}$$

where $\varepsilon_{s,max}$ is the solid volume fraction at maximum packing condition (which in this study was set equals to 0.60 using theoretical/experimental results by Fluent Inc. [38] and Yang [46]).

Figs. 2(a) and 2(b) show the plot of estimated particle cluster diameter and concentration with time-averaged solid particle concentration/volume fraction, which were calculated from various empirical literature correlations, respectively. The graph line results were for the CFB riser condition and the symbol results were for the CFB downer condition. All the empirical correlations showed similar trends of estimated values. The particle cluster diameter and concentration were directly increased with the increasing of solid particle concentration/volume fraction. These tendencies were consistent with the experimental data observed by many researchers [32-35]. As the higher quantity of solid particle, the probability of agglomeration or accumulation of solid particles as particle clusters is increased. This explains the observed trends as shown in the figures.

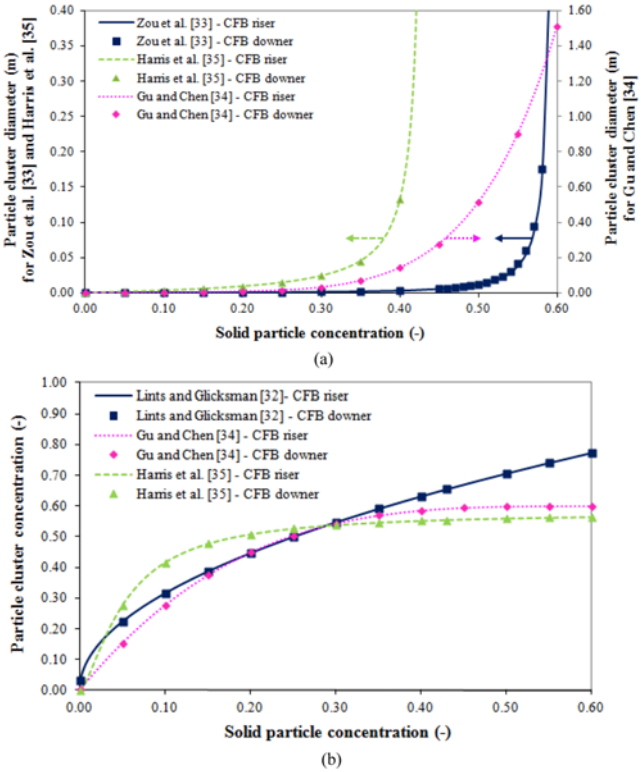

Fig. 2. Particle cluster (a) diameter and (b) concentration estimated from various empirical literature correlations.

4. Observation of Particle Cluster Inside CFB Riser and Downer

The CFD model, which was already verified in our previous studies [12,39], was used as a method for verifying the obtained results. It is then suitable for analyzing more information on CFB riser and downer systems. In this section, the system flow structures in both CFB riser and downer are shown. The calculation methodologies in the previous sections were then used to compute the particle cluster diameters and concentrations. Lastly, the computed results between the CFB riser and downer and with the estimated values from the literature empirical correlations were compared [32-35].

4-1. Demonstration of Particle Cluster Flow Structure

Fig. 3 illustrates the snapshots of computed instantaneous solid volume fraction distribution in the CFB riser at six different simulation times (which were 0 s, 10 s, 20 s, 30 s, 40 s and 50 s). The results were captured between the system heights of 3.50 m to 10.50 m. This CFB riser part is the center part in which the system is operated in the fully developed condition. At the top and bottom regions of the figure, the results thus were similar. From the contour color scale, the dense core-annulus flow structure was observed. The red color means high solid volume fraction condition, while the blue color means low solid volume fraction condition. More downward flow of solid particles can be seen near the wall region than at the center region of the CFB riser. This is similar to the results with this experi-

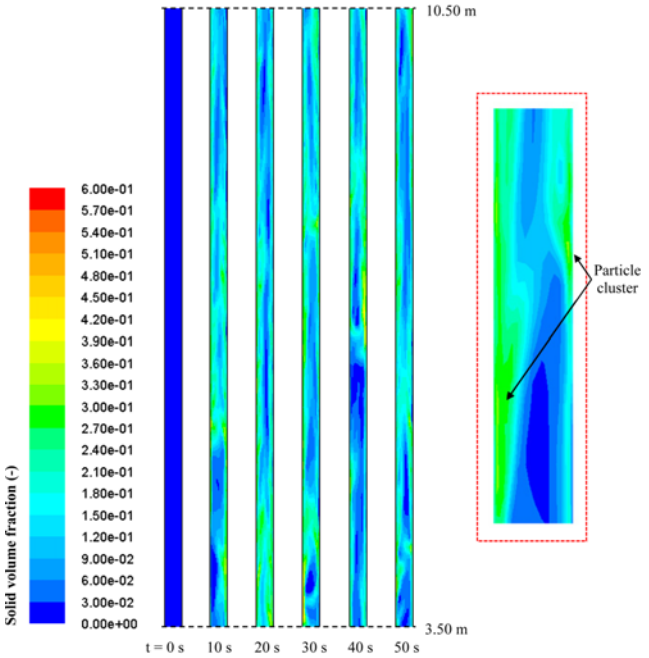

Fig. 3. Snapshots of computed instantaneous solid volume fraction distribution in the CFB riser at six different simulation times.

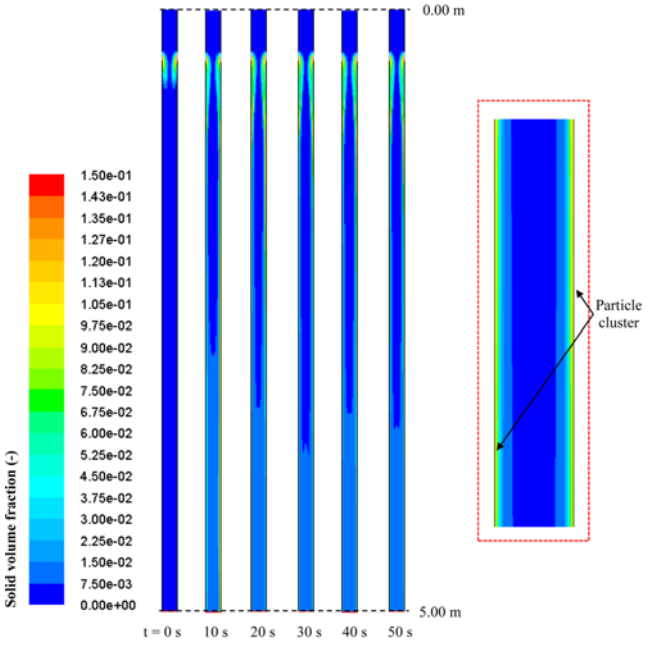

Fig. 4. Snapshots of computed instantaneous solid volume fraction distribution in the CFB downer at six different simulation times.

mental system condition [12,36]. About the particle cluster information, we observed that some system area had significantly stronger contour color than the other system area. This implies the occurrence of the particle cluster inside the system. The particle cluster had heterogeneity movements. It can fall down, move up, stagnate, break and agglomerate inside system, which is consistent with the previous literature results [21-24]. However, from the expanded figure, it could be clearly seen that particle clusters occurred mostly near the wall region. The particle cluster concentration or volume fraction was about 0.40 with the particle cluster diameter of approximately 0.01 m. In the figure, the appropriate time-averaged range was also confirmed. The results after 30 s were not changed with the simulation

Table 3. The computed information on particle cluster diameters at various different heights of the CFB riser and downer

CFB riser				
Height (m)	Dimensionless system height (-)	Radial solid dispersion coefficient (m^2/s)	Radial oscillating velocity (m/s)	Particle cluster diameter (m)
1.50	0.11	5.28E-03	2.52E-01	1.73E-02
3.50	0.25	2.47E-03	2.24E-01	1.01E-02
5.50	0.39	2.73E-03	2.80E-01	8.43E-03
7.00	0.49	2.76E-03	2.59E-01	9.52E-03
8.50	0.60	2.25E-03	2.19E-01	8.75E-03
10.50	0.74	2.46E-03	2.43E-01	8.73E-03
12.50	0.88	1.61E-03	1.46E-01	1.01E-02
Averaged		2.79E-03	2.32E-01	1.04E-02
CFB downer				
Height (m)	Dimensionless system height (-)	Radial solid dispersion coefficient (m^2/s)	Radial oscillating velocity (m/s)	Particle cluster diameter (m)
1.00	0.20	9.66E-07	1.07E-03	9.02E-04
2.00	0.40	4.83E-07	7.31E-04	6.60E-04
3.00	0.60	2.68E-07	5.60E-04	4.80E-04
4.00	0.80	3.62E-08	2.48E-04	1.46E-04
5.00	1.00	1.32E-07	5.07E-04	2.60E-04
Averaged		3.77E-07	6.23E-04	4.90E-04

time. Therefore, the 30 s to 50 s was selected as the time-averaged range in the following sections.

The snapshots of computed instantaneous solid volume fraction distribution in the CFB downer at similar six different simulation times are displayed in Fig. 4. The results are shown throughout the system heights between 0.00 m to 5.00 m. At the top and bottom regions of the figure, the results thus were not the same. This is due to the inlet and outlet system configurations. At the center region, the fully developed distribution was approximately constant. From the contour color scale, the dilute core-annulus flow structure was observed in the CFB downer. This is in agreement with the experimental observation in this system [37,39]. The high downward flow of solid particles near the wall region was obtained because the system moved with the same direction as gravitational acceleration. Similar to the CFB riser results, the formation of particle clusters in the CFB downer was also observed. However, the particle cluster, formed as a thin sheet near the wall, had less movement when compared to the CFB riser. Therefore, it could be implied that the particle cluster in CFB downer possessed less heterogeneity movements than that in the CFB riser. No particle cluster was moving upward inside the system, as can be seen from the expanded figure. For the particle cluster dynamics, its diameter in the downer was two-times smaller than the one in CFB riser, around 0.005 m, and its concentration was about 0.08.

4-2. Computation of Particle Cluster Diameter in CFB Riser and Downer

After the simulation results were obtained, the radial normal Reynolds stresses, the Lagrangian integral time scale, the radial solid dispersion coefficient and radial oscillating velocity were computed. Then, the particle cluster diameters were calculated using the proposed methodology together with the kinetic theory of granular flow concept. Table 3 summarizes the computed information on particle cluster diameter at various different heights of the CFB riser and downer. The results consisted of the time-averaged and area-averaged radial solid dispersion coefficient, radial oscillating velocity and particle cluster diameter. For the CFB riser, seven system heights were selected to show, ranging between 1.50 m to 12.50 m above the system inlet. For the CFB downer, five system heights were chosen to represent the system characteristics which were 1.00 m to 5.00 m below the system inlet. In the table, the averaged values from all the system heights are also shown. As for the radial dispersion coefficients, the values for the CFB riser were higher than the ones for the CFB downer approximately four orders of magnitude. As already discussed, this is because of more system heterogeneities in CFB riser or more stable flow structure in CFB downer. For the radial oscillating velocities, the computed values were consistent with the obtained radial solid dispersion coefficients. For the particle cluster diameters, the values from the CFB riser were larger than the ones from the CFB downer. These are similar to the observed flow structures in Figs. 3 and 4. Near the system inlet (bottom region in CFB riser/top region in CFB downer), both the values from CFB riser and downer were high. This is due to the agglomeration of the solid particles. At the center region, the particle cluster diameters were varied and decreased with the system heights. At the top region, the solid particle cluster diameters were slightly increased due to the solid particle accumulation at the outlet system configuration. However, it could be inferred that the computed values were approximately constant after the system reached the fully developed condition. The observed flow structures are clearly seen in Fig. 5, which displays the axial distributions of computed time-averaged and area-averaged particle cluster diameter in the CFB (a) riser and (b) downer.

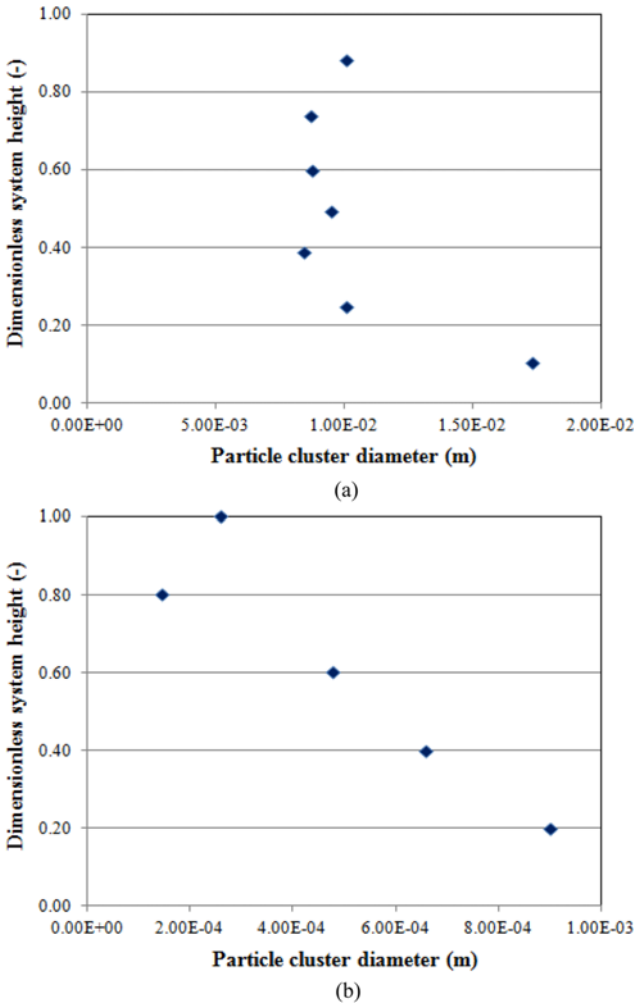

Fig. 5. The axial distributions of computed time-averaged and area-averaged particle cluster diameter in the CFB (a) riser and (b) downer.

4-3. Computation of Particle Cluster Concentration in CFB Riser and Downer

In this section, the particle cluster concentration results are calculated based on the statistical methodology as already described. Fig. 6 illustrates the radial distributions of computed time-averaged and area-averaged (a) solid particle and (b) particle cluster concentrations at the same seven different CFB riser heights. The radial distributions of computed time-averaged and area-averaged (a) solid particle and (b) particle cluster concentrations at the same five different CFB downer heights are shown in Fig. 7. All the computation profiles showed a similar behavior to each other, but the particle cluster concentrations had higher values than the solid particle concentration. This is because the solid particles are combined together as the particle clusters. These results confirm the similar core-annulus flow structure in different system axial or vertical locations. For the radial distributions, both the solid particle and particle cluster con-

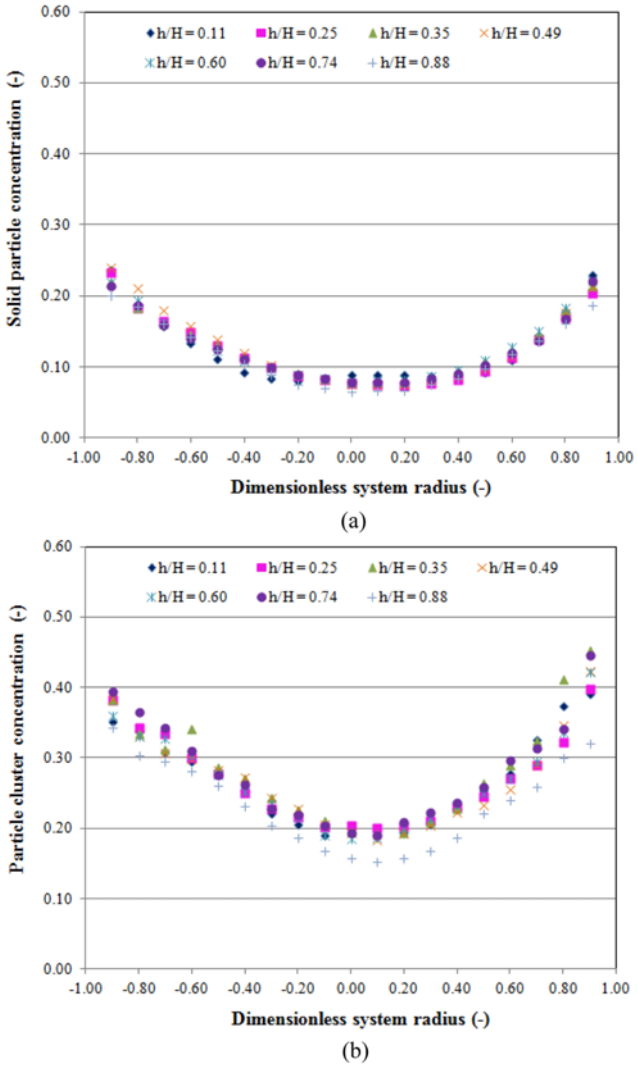

Fig. 6. The radial distributions of computed time-averaged and area-averaged (a) solid particle and (b) particle cluster concentrations at seven different CFB riser heights.

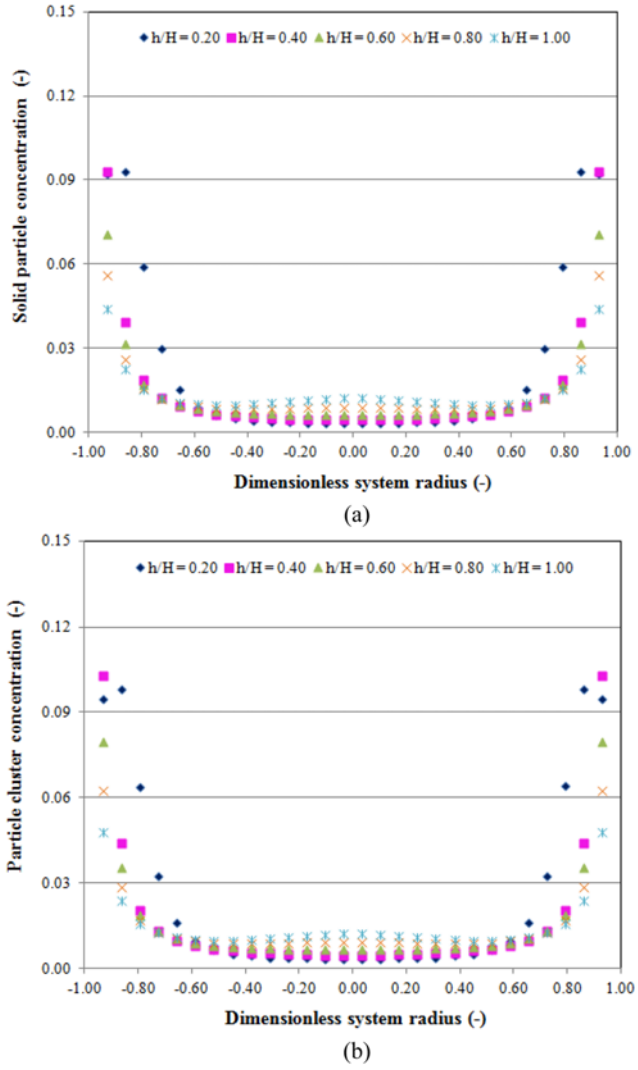

Fig. 7. Radial distributions of computed time-averaged and area-averaged (a) solid particle and (b) particle cluster concentrations at five different CFB downer heights.

centrations near the wall region were larger than the ones at the center region. When comparing between the CFB riser and downer, the values for the CFB riser were much larger than the CFB downer. This is because dense and dilute core-annulus flow structures were obtained in the CFB riser and downer, respectively. For the CFB riser, the values of particle cluster concentration at the wall region were approximately 0.32 to 0.45 which matched with the extracted value from Fig. 3. For the CFB downer, the particle cluster concentrations at the wall region were about 0.05 to 0.10, which is also consistent with the contour color in Fig. 4. These phenomena can be explained by the direction of system flow structure when comparing with the other force inside the system.

Fig. 8 shows the axial distributions of computed time-averaged and area-averaged solid particle and particle cluster concentrations in the CFB (a) riser and (b) downer. The selected system heights were similar to the ones in the previous figures. As already discussed, the selected CFB riser height were assumed to operate in the fully developed condition. It can be seen that the obtained solid particle and particle cluster concentrations were approximately the same in each system height. Therefore, these verified the proposed assumption. Due to the selected system heights, the solid particle and particle cluster concentrations in the CFB downer were varied. Thus, near the system inlet (top region), the solid particle and particle cluster concentrations were high. Then, the values were considered as slightly decreased or approximately constant when the system heights were increasing. This situation can be explained by the inlet configuration and the force balance inside the CFB downer. As the system height is increasing, the acceleration force inside the system is increased. In addition, the solid particle concentrations were higher than the particle cluster ones, similar to the obtained results in Figs. 6 and 7.

4-4. Comparisons of Particle Cluster Dynamics with the Empirical Correlations

After we identified and characterized the particle cluster dynamics, the comparisons with the literature empirical correlations [32-35] were shown. Table 4 shows the comparisons between the computed time-averaged particle cluster diameters and the previous empirical correlations [33-35] for the CFB riser and downer. In the table, the averaged values over system diameter and height are shown.

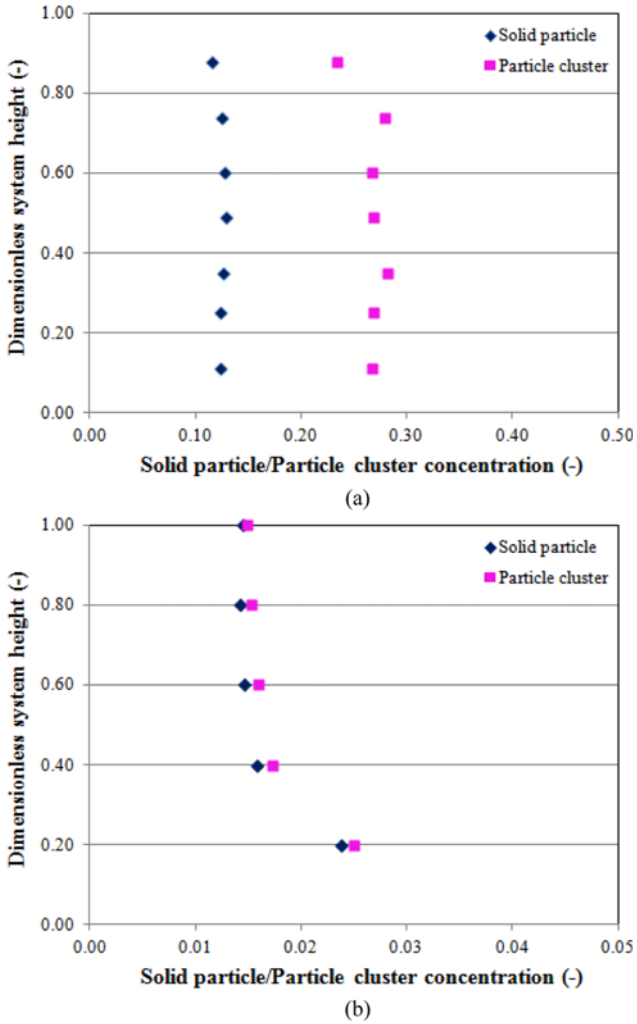

Fig. 8. Axial distributions of computed time-averaged and area-averaged solid particle and particle cluster concentrations in the CFB (a) riser and (b) downer.

From the calculation methodology in this study, the minimum and maximum values of particle cluster diameter ranged from 0.0001 m to 0.0173 m, respectively. As already discussed, the previous empirical correlations were only the curve fitting relation between the solid particle concentration/solid particle diameter and the particle cluster diameter. To get more precise information, the minimum and maximum values were computed. The minimum values were generally calculated based on the solid particle concentrations, while the maximum values were calculated based on the particle cluster concentrations. This was done because some previous researchers did not characterize the solid particle/particle cluster in their experiments. The measured concentrations then can both occur by individual solid particles and their agglomerate. Most of the calculated values in this study are in the range of the empirical correlations. This result can capture a realistic higher particle cluster diameter. Comparing between the CFB riser and downer, the values in CFB downer are more slightly deviated. This is because the experimental data, which were used to formulate the empirical correlations, were mostly operated in the CFB riser. However, the values were consistent with the roughly observed values in CFB downer by Bolkan et al. [47]; therefore, they are acceptable.

The comparisons between the computed time-averaged particle cluster concentrations and the previous empirical correlations [32,34,35] for the CFB riser and downer are also summarized in Table 4. The averaged values are shown for both at the wall and at the overall system. The particle cluster concentrations at the wall are higher than the ones at the overall system. For the comparison with the empirical correlations, only the computed values at the wall were employed. All the values from the previous correlations were both quantitatively and qualitatively in agreement with the values of this study. Similar to particle cluster diameter, the values in the CFB riser were more accurate than in CFB downer due to the available experimental data. However, all the results in this table confirm the validity of the calculation methodologies for particle cluster dynamics.

5. Explanation of Particle Cluster Dynamics Inside CFB Riser and Downer

Fig. 9 displays the snapshots of computed instantaneous solid velocity vectors in the CFB (a) riser and (b) downer at simulation time of 40 s. The results are shown both at all the system height and at the specific center section (fully developed system condition). After the system reached the fully developed condition, the

Table 4. The comparisons between the computed time-averaged particle cluster diameters and concentrations and the previous empirical correlations for the CFB riser and downer

Method/Correlation	Particle cluster diameter (m)			Method/Correlation	Particle cluster concentration (-)	
	Minimum	Maximum	Averaged		Wall	Averaged
CFB riser						
This study	0.0084	0.0173	0.0104	This study	0.3891	0.2667
Zou et al. [33]	0.0031	0.0097	0.0060	Lints and Glicksman [32]	0.3532	-
Gu and Chen [34]	0.0031	0.0225	0.0106	Gu and Chen [34]	0.3283	-
Harris et al. [35]	0.0039	0.0200	0.0108	Harris et al. [35]	0.4519	-
CFB downer						
This study	0.0001	0.0009	0.0005	This study	0.0872	0.0220
Zou et al. [33]	0.0002	0.0002	0.0002	Lints and Glicksman [32]	0.1437	-
Gu and Chen [34]	0.0011	0.0013	0.0012	Gu and Chen [34]	0.0677	-
Harris et al. [35]	0.0005	0.0007	0.0006	Harris et al. [35]	0.1154	-

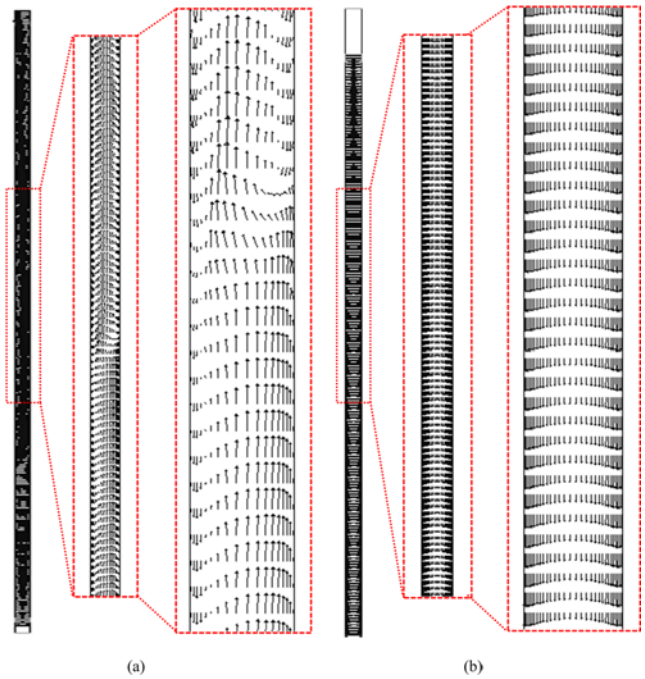

Fig. 9. Snapshots of computed instantaneous solid velocity vectors in the CFB (a) riser and (b) downer at simulation time of 40 s.

profiles were approximately constant. In the CFB riser, the results confirmed the heterogeneity movement as observed in this study and in other literature publications [21-24]. The solid velocity mostly moved up at the center and fell at the wall region. At the wall region, the solid velocity vectors were longer (higher velocity values) as the system height decreasing. This implies that accumulation of particle cluster had occurred. The breakage of particle cluster was also observed in the expanded figure. At that system point, the solid velocity vector changed its flow direction. This type of particle cluster is type I as proposed by Zhang et al. [25]. They proposed that there are two types of particle clusters in a CFB riser and downer. The particle cluster type I occurred at the near wall region where the solid velocities are low, and the particle cluster type II occurred in the center region where the solid velocities are high. However, the particle cluster type II can also be observed by the contour color in Fig. 3. In the CFB downer, the profiles were more stable. The particle cluster moved downward along with the gravitational acceleration. Similar to the CFB riser, both particle cluster types were observed with very low concentrations, though most of them were particle cluster type I with lower downward solid velocity than at the center region. About the difference between particle cluster behavior between CFB riser and downer, the velocities of some type I particle clusters in the CFB riser were downward and opposite to the main flow direction, but the velocities of all type I particle clusters in the CFB downer were downward and the same as the main flow direction. Therefore, back mixing due to particle cluster in the near wall region of a CFB downer did not occur. In addition, it can be implied that the duration time for the particle cluster in the CFB riser is longer than that in the CFB downer, which is qualitatively consistent with the experimental result by Zhang et al. [48]. About the explanation why the particle clusters were formed, it could be clarified by the solid particle force balance inside each system [2, 49]. This phenomenon is probably due to the mixed effect of drag force, gravity force, wall resistance, solid particle properties and multiphase turbulence. For an example application of the computed particle cluster dynamics, the Sherwood numbers or dimensionless number describing mass transfer were computed using the particle cluster diameter with the methodology in Chalermsinsuwan et al. [12]. The obtained results confirmed the low Sherwood numbers, which were 0.01 in CFB riser and 0.33 in CFB downer. This is due to the particle cluster formation inside the system. Then, this knowledge can be further used as criteria for designing of CFB reactor application such as selecting the appropriate chemical reaction sides for each reaction in chemical looping.

CONCLUSION

The information of particle cluster diameters and concentrations is useful for improving the performance of a circulating fluidized bed (CFB) system. These aggregates play a major role in flow development length, axial and radial dispersions near the wall and mass and heat transfers near the wall as well. In the literature, the way to identify and characterize the important parameters of particle cluster, diameter and concentration, is in a development stage for use in the computational fluid dynamics simulation (CFD) aspect.

This study calculated the particle cluster diameters and concentrations from two-dimensional CFD simulation results by using the concepts of kinetic theory of granular flow and statistic. The mathematical models were already verified with the CFB riser and downer experimental data in our previous study and thus used for computing the particle cluster dynamics. In the CFB riser, a dense core-annulus flow structure was observed, while in the CFB downer, a dilute core-annulus flow structure was obtained. The particle cluster in the CFB riser had more heterogeneity movements than that in the CFB downer, which could be explained by the system flow direction. About the particle cluster dynamics, the particle cluster diameters and concentrations in the CFB riser were higher than in the CFB downer. The particle cluster dynamics were increased with decreasing system height, due to the accumulation of solid particles. Then, the obtained values were compared with the predicted values from the empirical correlations. Most of the values were in the range of the empirical correlations, which confirmed the validity of the calculation methodology. Finally, the particle cluster dynamics and example application inside the CFB riser and downer were discussed.

These simulation results reveal the power of the CFD simulation application. Still, the computer capacity remains the limitation for simulating a complex system. Although the two-dimensional model is proven to represent the three-dimensional system in this study, the three-dimensional model is more realistic than the two-dimensional model with higher computational effort.

NOMENCLATURE

General Letters

C_{D0} : drag coefficient [-]
$\bar{d}_{cl}$: particle cluster diameter [m]
d_p : solid particle diameter [m]
D_x : radial solid dispersion coefficient [m^2/s]

e : restitution coefficient between solid particles [-]
e_W : restitution coefficient between solid particle and wall [-]
g : gravity force [m/s^2]
g_0 : radial distribution function [-]
G : mass flux [kg/m^2 s]
h : height of system [m]
H : overall height of system [m]
I : unit tensor [-]
m : total number of particle clusters [-]
n : unit vector [-]
p : pressure [Pa]
r : radial direction [-]
Re_k : Reynolds number [-]
T_L : lagrangian integral time scale [s]
t : time [s]
v : velocity vector [m/s]
v′ : velocity fluctuation [m/s]
$v_{s,slip}$: slip velocity of solid particle at the wall [m/s]
$v_{s,W}$: velocity of solid particle at the wall [m/s]
$v_{t,W}$: tangential velocity of solid particle at the wall [m/s]
x : radial or horizontal distance [m]
y : axial or vertical distance [m]

Greek Letters

β_{gs} : drag or interphase exchange coefficient [kg/m^3 s]
ε, $\overline{\varepsilon}$: volume fraction [-]
$\overline{\varepsilon}_{cl}$: solid volume fraction of particle cluster [-]
ε_{mf} : solid volume fraction at minimum fluidization velocity [-]
$\varepsilon_{s,max}$: solid volume fraction at maximum packing [-]
ϕ : specularity coefficient [-]
γ_s : collisional dissipation of solid fluctuating energy [kg/m s^3]
κ_s : conductivity of the solid fluctuating energy [kg/ m s]
μ : viscosity [kg/m s]
θ : granular temperature [m^2/s^2]
ρ : density [kg/m^3]
σ : standard deviation [-]
τ : stress tensor [Pa]
ξ : bulk viscosity [kg/m s]

Subscripts

g : gas phase
s : solid phase

ACKNOWLEDGEMENTS

This study was financially supported by grants from the Thailand Research Fund (TRF) and the Commission on the Higher Education for fiscal year 2012-2014 (MRG5580140), the Grant for Development of New Faculty Staff (Ratchadaphisek Somphot Endowment Fund) of Chulalongkorn University and the Center of Excellence on Petrochemical and Materials Technology, Chulalongkorn University.

REFERENCES

1. S. Benyahia, H. Arastoopour, T. M. Knowlton and H. Massah, *Powder Technol.*, **112**, 24 (2000).
2. Y. Cheng, C. Wu, J. Zhu, F. Wei and Y. Jin, *Powder Technol.*, **183**, 364 (2008).
3. B. Chalermsinsuwan, P. Kuchonthara and P. Piumsomboon, *Chem. Eng. Process.*, **49**, 1144 (2010).
4. B. Chalermsinsuwan, P. Piumsomboon and D. Gidaspow, *Chem. Eng. Sci.*, **64**, 1212 (2009).
5. T. McKeen and T. Pugsley, *Powder Technol.*, **129**, 139 (2003).
6. J. Wang, W. Ge and J. Li, *Chem. Eng. Sci.*, **63**, 1553 (2008).
7. M. T. Shah, R. P. Utikar, M. O. Tade, V. K. Pareek and G. M. Evans, *Chem. Eng. Sci.*, **66**, 3291 (2011).
8. D. Gidaspow and J. Veeraya, *J. Power Sources*, **166**, 400 (2007).
9. O. Levenspiel, *Chemical reaction engineering*, John Wiley & Sons, New York (1999).
10. R. W. Breault, *Powder Technol.*, **163**, 9 (2006).
11. M. Kashyap and D. Gidaspow, *Powder Technol.*, **203**, 40 (2010).
12. B. Chalermsinsuwan, P. Piumsomboon and D. Gidaspow, *Chem. Eng. Sci.*, **64**, 1195 (2009).
13. K. Tuzla, A. K. Sharma, J. C. Chen, T. Schiewe, K. E. Wirth and O. Molerus, *Powder Technol.*, **100**, 166 (1998).
14. E. Helland, R. Occelli and L. Tadrist, *Int. J. Multiphas. Flow*, **28**, 199 (2002).
15. J. X. Zhu, Z. Q. Yu, Y. Jin, J. R. Grace and A. Issangya, *Can. J. Chem. Eng.*, **73**, 662 (1995).
16. S. V. Manyele, J. H. Parssinen and J. X. Zhu, *Chem. Eng. J.*, **88**, 151 (2002).
17. R. W. Breault, C. J. Ludlow and P. C. Yue, *Powder Technol.*, **149**, 68 (2005).
18. J. W. Chew, R. Hays, J. G. Findlay, T. M. Knowlton, S. B. R. Karri, R. A. Cocco and C. M. Hrenya, *Chem. Eng. Sci.*, **68**, 72 (2012).
19. J. Yerushalmi, N. T. Cankurt, D. Geldart and B. Liss, *AIChE Symp. Ser.*, **74**, 1 (1976).
20. D. Gidaspow, Y. P. Tsuo and K. M. Luo, *Computed and experimental cluster formation and velocity profiles in circulating fluidized beds*, Fluidization IV, Alberta, Canada (1989).
21. M. Horio and H. Kuroki, *Chem. Eng. Sci.*, **49**, 2413 (1994).
22. M. Tartan and D. Gidaspow, *AIChE J.*, **50**, 1760 (2004).
23. J. Jung, D. Gidaspow and I. K. Gamwo, *Ind. Eng. Chem. Res.*, **44**, 1329 (2005).
24. J. Xu and J. X. Zhu, *Chem. Eng. J.*, **168**, 376 (2011).
25. M. H. Zhang, K. W. Chu, F. Wei and A. B. Yu, *Powder Technol.*, **184**, 151 (2008).
26. C. Soong, K. Tuzla and J. Chen, *Identification of particle clusters in circulating fluidized bed*, Circulating Fluidized Bed Technology Vol. IV, New York, USA (1995).
27. A. Sharma, K. Tuzla, J. Matsen and J. Chen, *Powder Technol.*, **111**, 114 (2000).
28. L. C. Gómez, R. C. da Silva, H. A. Navarro and F. E. Milioli, *Appl. Math. Model.*, **32**, 327 (2007).
29. D. Gidaspow, *Multiphase flow and fluidization: Continuum and kinetic theory description*, Academic Press, Boston (1994).
30. R. W. Breault, *Powder Technol.*, **220**, 79 (2012).
31. C. Guenther and R. Breault, *Powder Technol.*, **173**, 163 (2007).
32. M. Lints and L.R. Glicksman, *AIChE Symp. Ser.*, **89**, 35 (1993).
33. B. Zou, H. Li, Y. Xia and X. Ma, *Powder Technol.*, **78**, 173 (1994).
34. W. K. Gu and J. C. Chen, *A model for solid concentration in circulating fluidized beds*, Fluidization X., Durango, Colorado, USA (1998).

35. A. T. Harris, J. F. Davidson and R. B. Thorpe, *Powder Technol.*, **127**, 128 (2002).
36. T. Knowlton, D. Geldart, J. Masten and D. King, *Comparison of CFB hydrodynamic models*, PSRI Challenge Problem Presented at the Eighth International Fluidization Conference, Tours, France (1995).
37. C. Cao and H. Weinstein, *AIChE J.*, **46**, 515 (2000).
38. Fluent Inc., *Fluent 6.2 User's Guide*, Fluent Inc., Lebanon (2005).
39. B. Chalermsinsuwan, T. Chanchuey, W. Buakhao, D. Gidaspow and P. Piumsomboon, *Chem. Eng. J.*, **189-190**, 313 (2012).
40. B. Sun and D. Gidaspow, *Ind. Eng. Chem. Res.*, **38**, 787 (1999).
41. N. Yang, W. Wang, W. Ge and J. Li, *Chem. Eng. J.*, **96**, 71 (2003).
42. B. Chalermsinsuwan, P. Kuchonthara and P. Piumsomboon, *Chem. Eng. Process.*, **48**, 165 (2009).
43. S. Benyahia, H. Arastoopour and T. M. Knowlton, *Chem. Eng. Commun.*, **189**, 510 (2009).
44. P. C. Johnson and R. Jackson, *J. Fluid Mech.*, **176**, 67 (1987).
45. V. Jiradilok, D. Gidaspow and R. W. Breault, *Chem. Eng. Sci.*, **62**, 3397 (2007).
46. W. C. Yang, *Handbook of fluidization and fluid-particle systems*, Marcel Dekker, Inc., New York (2003).
47. Y. Bolkan, F. Berruti, J. Zhu and B. Milne, *Powder Technol.*, **132**, 85 (2003).
48. M. H. Zhang, Z. Qian, H. Yu and F. Wei, *Powder Technol.*, **129**, 46 (2003).
49. Y. Zhao, Y. Ding, C. Wu and Y. Cheng, *Powder Technol.*, **199**, 2 (2010).